Relative Intensity Noise of Silicon Hybrid Laser

Xiao Nan Hu, Tao Liu, Yu Lian Cao, Bo Meng, Hong Wang, Geok Ing Ng, Xian Shu Luo, Tsung Yang Liow, Jun Feng Song, Guo Qiang Lo, *Member, IEEE*, and Qi Jie Wang, *Senior Member, IEEE*

***Abstract*— We theoretically investigate the relative intensity noise (RIN) of a silicon hybrid laser by taking into account two-dimension transverse modes in the hybrid waveguide. It shows that, when only one transverse mode is excited, RIN spectrum of the hybrid laser exhibits a larger peak value at a lower relaxation oscillation (RO) frequency as compared with the case of a conventional multiple-quantum well (MQW) laser with the the same active region design and dimension. In contrast, when two transverse modes are excited, the hybrid laser shows a lower peak value at a higher RO frequency as compared with the MQW laser. The effects of waveguide dimensions, e.g., Si ridge height and III–V ridge width on RIN spectra of the hybrid laser are also investigated.**

***Index Terms*— Relative intensity noise (RIN), semiconductor laser, silicon photonics, transverse modes.**

I. Introduction

THE on-going rapid development of microprocessor chips is facing several challenges, e.g., limited bandwidth, capacity and heat dissipation. To overcome these challenges, there are tremendous interests in developing silicon-on-insulator (SOI) platforms to replace the current electrical interconnects and networks with optical counterparts. Although SOI amplifiers [1], modulators [2], and detectors [2] have already been demonstrated on SOI platforms, optical lasing from silicon becomes a bottleneck to fully realize this platform due to its intrinsic indirect bandgap. Optically pumped Raman lasers [3], rare-earth doped Si rich oxides lasers [4], etc. have been demonstrated in silicon, but they could not fully act as transmitters in the platform because of their restricted performance and operation conditions. Recently, an electrically pumped silicon hybrid laser has been demonstrated based on wafer-to-wafer bonding techniques [5]. This hybrid laser is constructed by the integration of III-V epitaxial wafers on SOI wafers, followed by standard photolithograph and etching processes to define the device structure. The advantages of large-scale low-cost integration and relaxed alignment requirements make it a suitable candidate for the platform. With similar technology and concepts, other devices, e.g., racetrack [6], distributed feedback (DFB) [7], mode-locked silicon hybrid laser [8], [9] and amplifier [10] as well as detector [11], are also successfully demonstrated.

To be a promising and reliable candidate for the platform, a hybrid laser with excellent noise performance is highly desired. As one of the noise sources, relative intensity noise (RIN) is an important indicator for intensity stability of devices. A low RIN results in a low error rate in optical data communication, and the relaxation oscillation (RO) frequency derived from the RIN spectrum shows an associated theoretical maximum modulation bandwidth of the device [12]. A lot of works are devoted to RIN analysis. For instance, the effect of the number of quantum wells as well as associated differential gain, etc. on the RIN of multiple-quantum-well (MQW) lasers has been investigated [13], and a much lower peak value of RIN below -157dB/Hz has been reported for MQW lasers [14]. Although many efforts were made on the study of intrinsic frequency response of MQW lasers, there is no detailed study of such dynamics or experimental report in the new-developed silicon hybrid lasers.

In the hybrid laser, two waveguides are put together closely: one is the III-V region which provides the gain, and the other is the SOI region which transmits light to subsequent devices in the platform. Therefore, its cavity mode profile has to be described in two-dimension transverse plane. As far as we know, the waveguide dimension can strongly influence the coupled mode profile in hybrid lasers. This hybrid mode characteristic is different from that in conventional MQW lasers. Since it is reported that the mode distribution has a great influence on the RIN of a laser in MQW lasers [15], a hybrid laser is predicted to have a different RIN characteristic from the conventional MQW laser. Therefore, a study on RIN in hybrid lasers including two-dimension profiles is necessary.

In this manuscript, we extend the RIN calculation model by incorporating two-dimension transverse profiles and investigate on the RIN of a hybrid laser, for the first time, to theoretically show its intrinsic frequency response. The manuscript is organized as follows: in section II we simulate the optical mode in our considered cavity of hybrid lasers. And then, in section III, we present a theoretical model for the RIN analysis by considering two-dimension transverse modes.

Manuscript received October 27, 2013; revised February 5, 2014 and March 25, 2014; accepted March 29, 2014. Date of publication April 4, 2014; date of current version May 2, 2014. This work was supported in part by the A*STAR, under Grant 112 280 4038, and in part by the CNRS International-NTU-Thales Research Alliance (CINTRA) Laboratory, UMI 3288, Singapore 637553.

X. N. Hu, T. Liu, Y. L. Cao, B. Meng, H. Wang, and G. I. Ng are with NOVITAS, School of Electrical and Electronic Engineering, Nanyang Technological University, Singapore 639798 (e-mail: huxi0011@e.ntu.edu.sg; tliu1@e.ntu.edu.sg; caoyl@ntu.edu.sg; bmeng1@e.ntu.edu.sg; ewanghong@ntu.edu.sg; eging@ntu.edu.sg).

X. S. Luo, T. Y. Liow, J. F. Song, and G. Q. Lo are with the Institute of Microelectronics, Agency for Science, Technology and Research, Singapore 117685 (e-mail: luox@ime.a-star.edu.sg; liowty@ime.a-star.edu.sg; songjf@ime.a-star.edu.sg; logq@ime.a-star.edu.sg).

Q. J. Wang is with NOVITAS, School of Electrical and Electronic Engineering, Nanyang Technological University, Singapore 639798, and also with the Centre for Disruptive Photonic Technology, School of Physical and Mathematical Sciences, Nanyang Technological University, Singapore 637371 (e-mail: qjwang@ntu.edu.sg).

Color versions of one or more of the figures in this paper are available online at http://ieeexplore.ieee.org.

Digital Object Identifier 10.1109/JQE.2014.2315212

0018-9197 © 2014 IEEE. Personal use is permitted, but republication/redistribution requires IEEE permission.
See http://www.ieee.org/publications_standards/publications/rights/index.html for more information.

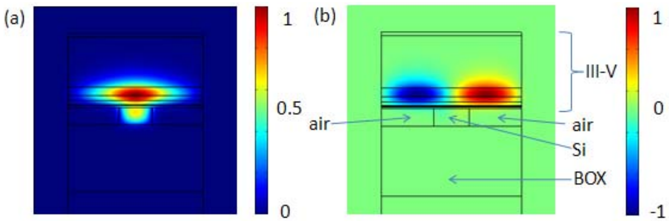

Fig. 1. The optical field distributions of the TE_{00} (a) and TE_{10} (b) mode of a hybrid laser with a 4μm-wide III-V ridge, a 1μm-wide and 500 nm-high Si ridge with arrows indicating the silicon-on-insulator (SOI) structure. BOX in (b) refers to buried oxide.

In section IV, both steady state and small signal modulation scenarios are analyzed. In section V, the RIN spectra of hybrid lasers are compared in terms of different dimensions e.g., III-V ridge widths and Si ridge heights. The comparison between a hybrid laser and a MQW laser is also discussed. Finally, we summarize the result.

II. Transverse Mode in Hybrid Laser

Silicon hybrid laser is a coupled waveguide structure, which comprises vertically a top active III-V waveguide providing the optical gain, and an underneath passive SOI waveguide transmitting light to other components on SOI. The SOI waveguide consists of Si ridge, buried oxide (BOX) layer and Si substrate. BOX thickness is fixed at 2 μm to prevent the coupling of light into Si substrate. When the III-V and SOI waveguides are designed to be evanescently coupled with homogenous width, a higher confinement in SOI will lead to a higher threshold current density due to a lower confinement in III-V active region. Although taper design could be used to improve the threshold performance [16], it is beyond the scope of this manuscript and only evanescent coupling is considered in our computation.

Typical TE_{00} mode and TE_{10} even supermode [17] are shown in Fig. 1 with a relatively large confinement in active region. The III-V material structure consists of an InAlGaAs-based MQW sandwiched by asymmetric InP cladding layers to couple more light into SOI waveguide, with reference to [5]. It is found that the TE_{10} mode has a larger confinement in active region than that of the TE_{00} mode due to no lateral carrier confinement in the III-V ridge. In the following model, we will investigate the effects of these two modes on the RIN. We assume uniform current injection over the entire III-V ridge without injection carrier confinement within the ridge. Current leakage from sidewalls is also ignored as the optical profile is independent on it. In addition, under some certain dimensions, TE_{10} mode will be excited first due to larger confinement in active region and moderate mode loss as compared to TE_{00} mode. To avoid this, the confinement in active region for the TE_{00} mode is maintained above 6% by controlling the hybrid laser structure in our calculation to ensure that the TE_{00} mode will be excited first. It is noted that the TE_{10} mode cannot be coupled into SOI, thus could not transmit into subsequent devices in the circuit. In the below discussion, we only focus on the RIN of the TE_{00} mode.

III. Two-Dimension Spatial-Temporal Model

The model extended in this manuscript includes both spatial dependence of the carrier and the optical field profile, hence the electric field can be expressed as

$$E(x, y, t) = \frac{1}{2}\sum_i \varphi_i(x, y)E_i(t)e^{-i\omega_i t} + cc. \qquad (1)$$

where $E_i(x, y)$, $\psi_i(x, y)$ and ω_i are the complex field amplitude, optical field profile, and angular velocity of the *ith* transverse mode, respectively, and cc. refers to the complex conjugate of the first term. In this manuscript, we consider DFB silicon hybrid laser at 1.55μm with a normal ridge-air facet. Only up to the first two transverse modes are excited and $\psi_i(x, y)$ is obtained from two-dimension simulations.

The time evolution of the carrier distribution within III-V ridge can be expressed as [15]

$$\frac{\delta N_i(x, y, t)}{\delta t} = D_n\nabla_r^2 N_i(x, y, t) - \frac{N_i(x, y, t)}{\tau_n} + \frac{j}{ed} - \sum_j \frac{v_g\tau_i}{d\overline{\psi_j(x, y)}^2}\psi_j^2(x, y)g_j(t)P_j(t) \qquad (2)$$

where $N_i(x, y)$, D_n, τ_n, v_g, τ_i, j, d, g_j, P_j are carrier density profile associated with ith mode, electron diffusion constant, electron lifetime, group velocity, ith mode confinement factor in active region, injection current density, total quantum wells thickness (including barriers), *jth* mode gain and the number of photons in *jth* mode, respectively.

$\overline{\psi_j(x, y)}^2$ is the *jth* mode average optical profile and can be written as

$$\overline{\psi_j(x, y)}^2 = \int_0^{L_1}\int_0^{L_2} \psi_j^2(x, y)dxdy \qquad (3)$$

where L_1, L_2 are III-V ridge height and width, respectively.

The rate equation for the photon number can be expressed as

$$\frac{dP_i(t)}{dt} = \left[v_g\tau_i g_i(t) - \frac{1}{\tau_{p,i}}\right]P_i(t) + \frac{d\beta\int_0^{L_1}\int_0^{L_2}N_i(x, y, t)dxdy}{\tau_n} + \sqrt{\frac{d\beta\int_0^{L_1}\int_0^{L_2}N_i(x, y, t)dxdy}{\tau_n}}\xi_i(t) \qquad (4)$$

where $\tau_{p,i}$, β are *ith* mode photon lifetime, and spontaneous emission factor, respectively. The last term in (4) represents the noise component and $\xi_i(t)$ is a real Gaussian noise term of zero mean, whose time correlation is given as $<\xi_i(t)\xi_j(s)> = 2\delta_{ij}\delta(t - s)$ [15]. In addition, there is a relationship between the carrier density and the gain as

$$g_i(t) = \frac{\int_0^{L_1}\int_0^{L_2} \psi_i^2(x, y)A[N_i(x, y, t) - N_0]dxdy}{\overline{\psi_i(x, y)}^2} \qquad (5)$$

where A is the differential gain and N_0 is transparent carrier density. Here we assume the laser is operated under normal condition where there is no gain saturation.

$$\overline{N_i(x,y)} = 4\sum_{m=1}^{\infty}\sum_{n=1}^{\infty}\int_0^{L_1}\int_0^{L_2} \sin\left(\frac{m\pi}{L_1}x\right)\sin\left(\frac{n\pi}{L_2}y\right)\frac{\sin\left(\frac{m\pi}{L_1}x'\right)\sin\left(\frac{n\pi}{L_2}y'\right)}{D_nL_1L_2\left[-\left(\frac{m\pi}{L_1}\right)^2-\left(\frac{n\pi}{L_2}\right)^2-\frac{1}{D_n\tau_n}\right]} \times\left(-\frac{j}{ed}+\sum_j\frac{v_g\tau_i}{d\overline{\psi_j(x,y)}^2}\varphi_j^2(x',y')g_{oj}\overline{P_j}\right)dx'dy' \tag{6}$$

IV. Steady State and Small Signal Analysis

For intensity noise investigation, the above rate equations could be expanded around the steady state values for small signal analysis. Using the boundary condition that $N(0,y) = N(L_2,y) = N(x,0) = N(x,L_1) = 0$, the steady state carrier density $\overline{N_i(x,y)}$ can be solved by setting (2) and (4) to be equal to zero as (6) where g_{oj} is *jth* mode steady state gain and can be solved from the steady state of (4) (ignore second term which is very close to zero and noise average is zero) that

$$g_{oj} = \frac{1}{v_g\tau_j\tau_{p,j}} \tag{7}$$

Then (6) and (7) are substituted into (5) thus *ith* mode power could be solved. For the TE_{00} mode,

$$a_{11}\overline{P_1} = b_1 \tag{8}$$

where a_{11}, b_1 are expressed as

$$a_{11} = 4\sum_{m=1}^{\infty}\sum_{n=1}^{\infty}\int_0^{L_1}\int_0^{L_2}\psi_1^2(x,y)A \frac{\sin\left(\frac{m\pi}{L_1}x\right)\sin\left(\frac{n\pi}{L_2}y\right)}{\overline{\psi_1(x,y)}^2}dxdy \times\int_0^{L_1}\int_0^{L_2}\frac{\sin\left(\frac{m\pi}{L_1}x'\right)\sin\left(\frac{n\pi}{L_2}y'\right)}{D_nL_1L_2\left[-\left(\frac{m\pi}{L_1}\right)^2-\left(\frac{n\pi}{L_2}\right)^2-\frac{1}{D_n\tau_n}\right]} \frac{v_g\tau_1}{d}\varphi_1^2(x',y')g_{o1}dx'dy'$$

$$b_1 = \frac{\overline{\psi_1(x,y)}^2}{v_g\tau_1\tau_{p,1}} + AN_0\int_0^{L_1}\int_0^{L_2}\psi_1^2(x,y)dxdy -16A\sum_{m=1}^{\infty}\sum_{n=1}^{\infty}\int_0^{L_1}\int_0^{L_2} \times\frac{\psi_1^2(x,y)\sin\left(\frac{m\pi}{L_1}x\right)\sin\left(\frac{n\pi}{L_2}y\right)}{D_nL_1L_2\left[-\left(\frac{m\pi}{L_1}\right)^2-\left(\frac{n\pi}{L_2}\right)^2-\frac{1}{D_n\tau_n}\right]} \times\left(-\frac{j}{ed}\right)\left(\frac{L_1}{m\pi}\right)\left(\frac{L_2}{n\pi}\right)dxdy$$

If both TE_{00} and TE_{10} modes exist simultaneously, then we have

$$a_{11}\overline{P_1} + a_{12}\overline{P_2} = b_1 \tag{9a}$$

$$a_{21}\overline{P_1} + a_{22}\overline{P_2} = b_2 \tag{9b}$$

where a_{ij}, b_2 are (i = 1,2; j = 1,2)

$$a_{ij} = 4\sum_{m=1}^{\infty}\sum_{n=1}^{\infty}\int_0^{L_1}\int_0^{L_2}\psi_i^2(x,y)A \frac{\sin\left(\frac{m\pi}{L_1}x\right)\sin\left(\frac{n\pi}{L_2}y\right)}{\overline{\psi_j(x,y)}^2}dxdy \times\int_0^{L_1}\int_0^{L_2}\frac{\sin\left(\frac{m\pi}{L_1}x'\right)\sin\left(\frac{n\pi}{L_2}y'\right)}{D_nL_1L_2\left[-\left(\frac{m\pi}{L_1}\right)^2-\left(\frac{n\pi}{L_2}\right)^2-\frac{1}{D_n\tau_n}\right]} \frac{v_g\tau_j}{d}\varphi_j^2(x',y')g_{oj}dx'dy'$$

$$b_2 = \frac{\overline{\psi_2(x,y)}^2}{v_g\tau_2\tau_{p,2}} + AN_0\int_0^{L_1}\int_0^{L_2}\psi_2^2(x,y)dxdy -16A\sum_{m=1}^{\infty}\sum_{n=1}^{\infty}\int_0^{L_1}\int_0^{L_2} \times\frac{\psi_2^2(x,y)\sin\left(\frac{m\pi}{L_1}x\right)\sin\left(\frac{n\pi}{L_2}y\right)}{D_nL_1L_2\left[-\left(\frac{m\pi}{L_1}\right)^2-\left(\frac{n\pi}{L_2}\right)^2-\frac{1}{D_n\tau_n}\right]} \times\left(-\frac{j}{ed}\right)\left(\frac{L_1}{m\pi}\right)\left(\frac{L_2}{n\pi}\right)dxdy$$

In the above equations, m and n are odd numbers for b_1 and b_2, respectively.

The typical L-I curves of a hybrid laser are shown in Fig. 2, where L-I curves in III-V waveguide are also given (see Fig. 2b). Since TE_{10} mode cannot be coupled into SOI waveguide, we only have interests in TE_{00} mode for a hybrid laser. Although the TE_{10} mode is not coupled into the SOI waveguide, it will affect the RIN characteristics of the TE_{00} mode once it is excited. Noted that the calculated power, in linear regime, of the TE_{00} mode coupled into SOI waveguide and the threshold current density are slightly higher than experimental values reported in [7]. The small discrepancy is caused by uncertainties in the parameters chosen for calculations. In addition, there is a kink in the calculated L-I curve of the TE_{00} mode due to the existence of mode competition when the TE_{10} mode is excited.

For small signal analysis, time dependent terms are expanded around steady state values as

$$P_i(t) = \overline{P_i} + \Delta P_i(t) \tag{10a}$$

$$N_i(x,y,t) = \overline{N_i(x,y)} + \delta N_i(x,y,t) \tag{10b}$$

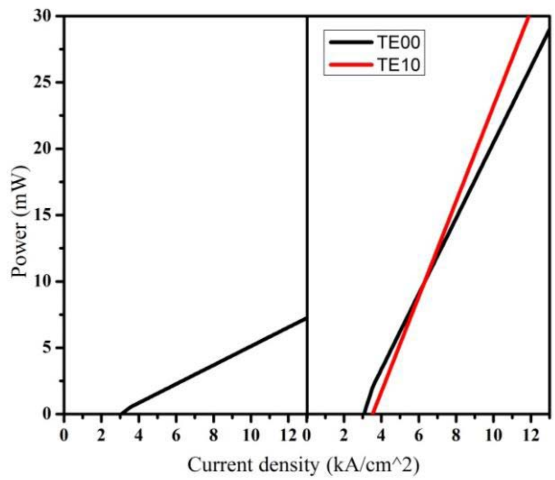

Fig. 2. The LI curves for a silicon hybrid laser (a) The LI curves in SOI waveguide where TE_{10} mode will not be coupled. (b) The LI curves in III-V waveguide where TE_{00} mode is excited first. The typical parameters used are: $L_1 = 2.196\mu$m, $D = 1\mathrm{cm}^2$/s, $A = 3.4 \times 10^{-16}\mathrm{cm}^2$, $N_0 = 8 \times 10^{17}\mathrm{cm}^{-3}$, $\upsilon_g = 0.75 \times 10^{10}$cm/s, $\tau_n = 2$ns, $\tau_{p,1} = 2.7$ps, $\tau_{p,2} = 2.5$ps, $\beta = 2 \times 10^{-5}$ taken from [13], [15].

$$\Delta g_i(t) = \frac{A\int_0^{L_1}\int_0^{L_2}\partial N_i(x,y,t)\psi_i^2(x,y)dxdy}{\overline{\psi_i(x,y)}^2} \quad (10c)$$

Therefore when (10) is substituted into (2) and (4), we obtain (neglect the second order perturbation terms and the diffusion perturbation)

$$\frac{\partial\delta N_i(x,y,t)}{\partial t} = -\frac{\delta N_i(x,y,t)}{\tau_n} - \sum_j \frac{\upsilon_g\tau_i}{d\overline{\psi_j(x,y)}^2}\psi_j^2(x,y)\left(\Delta g_j\overline{P_j} + g_{oj}\Delta P_j\right) \quad (11)$$

$$\frac{d\Delta P_i(t)}{dt} = v_g\tau_i\Delta g_i(t)\overline{P_i} + \sqrt{\frac{\overline{P_i}\beta d\int_0^{L_1}\int_0^{L_2}\overline{N_i(x,y)}dxdy}{\tau_n}}\xi_i(t) \quad (12)$$

If both sides of (11) multiply $A\psi_i^2(x,y)\Big/\overline{\psi_i(x,y)}^2$ and integrate over the entire III-V ridge, we obtain

$$\frac{d\Delta g_i(t)}{dt} = -\frac{\Delta g_i(t)}{\tau_n} - \sum_j \frac{A\upsilon_g\tau_i}{d\overline{\psi_j(x,y)}^2\,\overline{\psi_i(x,y)}^2} \times \left(\Delta g_j\overline{P_j} + g_{oj}\Delta P_j\right)\int_0^{L_1}\int_0^{L_2}\psi_j^2(x,y)\psi_i^2(x,y)dxdy \quad (13)$$

Similarly, for the TE_{00} mode,

$$\frac{d\Delta P_1(t)}{dt} = c_1\Delta g_1(t) + d_1\xi_1(t) \quad (14a)$$

$$\frac{d\Delta g_1(t)}{dt} = e_{11}\Delta g_1(t) + f_{11}\Delta P_1(t) \quad (14b)$$

where

$$c_1 = v_g\tau_1\overline{P_1}, d_1 = \sqrt{\overline{P_1}\beta d\int_0^{L_1}\int_0^{L_2}\overline{N_1(x,y)}dxdy\Big/\tau_n}$$

$$e_{11} = -\frac{1}{\tau_n} - \frac{A\upsilon_g\tau_1\int_0^{L_1}\int_0^{L_2}\psi_1^4(x,y)dxdy}{d\left[\overline{\psi_1(x,y)}^2\right]^2}\overline{P_1}$$

$$f_{11} = -\frac{A\upsilon_g\tau_1 g_{o1}\int_0^{L_1}\int_0^{L_2}\psi_1^4(x,y)dxdy}{d\left[\overline{\psi_1(x,y)}^2\right]^2}$$

If both TE_{00} and TE_{10} modes exist simultaneously, we obtain

$$\frac{d\Delta P_1(t)}{dt} = c_1\Delta g_1(t) + d_1\xi_1(t) \quad (15a)$$

$$\frac{d\Delta P_2(t)}{dt} = c_2\Delta g_2(t) + d_2\xi_2(t) \quad (15b)$$

$$\frac{d\Delta g_1(t)}{dt} = e_{11}\Delta g_1(t) + f_{11}\Delta P_1(t) + e_{21}\Delta g_2(t) + f_{21}\Delta P_2(t) \quad (15c)$$

$$\frac{d\Delta g_2(t)}{dt} = e_{12}\Delta g_1(t) + f_{12}\Delta P_1(t) + e_{22}\Delta g_2(t) + f_{22}\Delta P_2(t) \quad (15d)$$

where c_2, d_2, e_{ij}, f_{ij} are (i = 1,2; j = 1,2)

$$c_2 = \upsilon_g\tau_2\overline{P_1},\ d_2 = \sqrt{\overline{P_2}\beta d\int_0^{L_1}\int_0^{L_2}\overline{N_2(x,y)}dxdy\Big/\tau_n}$$

$$e_{ij} = -\frac{1}{\tau_n}\times\delta_{ij} - \frac{A\upsilon_g\tau_i\int_0^{L_1}\int_0^{L_2}\psi_i^2(x,y)\psi_j^2(x,y)dxdy}{d\overline{\psi_i(x,y)}^2\,\overline{\psi_j(x,y)}^2}\overline{P_i}$$

$$f_{ij} = -\frac{A\upsilon_g\tau_i g_{oi}\int_0^{L_1}\int_0^{L_2}\psi_i^2(x,y)\psi_j^2(x,y)dxdy}{d\overline{\psi_i(x,y)}^2\,\overline{\psi_j(x,y)}^2}$$

where δ_{ij} is Kronecker delta function.

Therefore, by solving (14) or (15), the RIN spectra could be obtained.

V. Results and Discussion

Once (14) and (15) are transformed into the frequency domain, $\Delta P_1(\omega)$ and $\Delta P_2(\omega)$ could be solved (the perturbation of diffusion is ignored). As defined in [18], RIN for the TE_{00} mode of a hybrid laser, is defined as

$$RIN_1 = 2\left\langle|\Delta P_1(\omega)|^2\right\rangle/\overline{P_1}^2 \quad (16)$$

where <·> refers to the mean values. For all calculations, Si ridge width is fixed at 1μm.

Figure 3 shows the RIN spectra of a hybrid laser at different injection currents, where the III-V ridge width is 3μm and the height of Si ridge is 220 nm. At $1.05\mathrm{J}_{\mathrm{th}}$, where J_{th} is the threshold current density, the laser only operates at the TE_{00} mode, while, under $1.4\mathrm{J}_{\mathrm{th}}$ and $1.8\mathrm{J}_{\mathrm{th}}$, the TE_{10} mode is excited. The frequency at peak of RIN spectrum corresponds to RO frequency, which is related to the theoretical largest modulation bandwidth [12]. At $1.05\mathrm{J}_{\mathrm{th}}$, the hybrid laser oscillates only at one RO frequency; but as two modes are excited, two RO frequencies appear, as shown in Fig. 3. Moreover, with the increase of the current, the RO frequency becomes blueshifted and the peak value of RIN decreases.

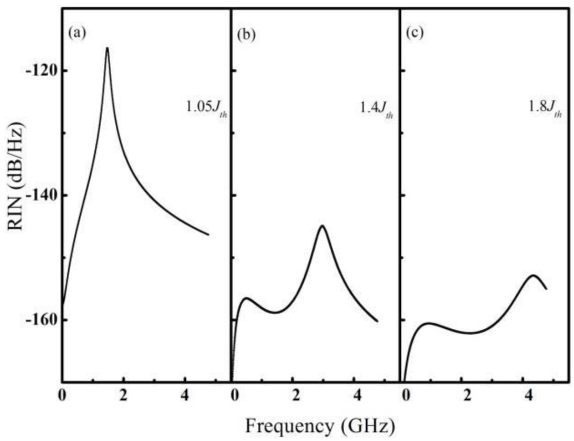

Fig. 3. The RIN spectra for hybrid laser with a 3μm III-V ridge width, 220 nm Si ridge height under different injection current density: (a) Injection current density is 1.05J_{th}; (b) Injection current density is 1.4J_{th}; (c) Injection current density is 1.8J_{th}.

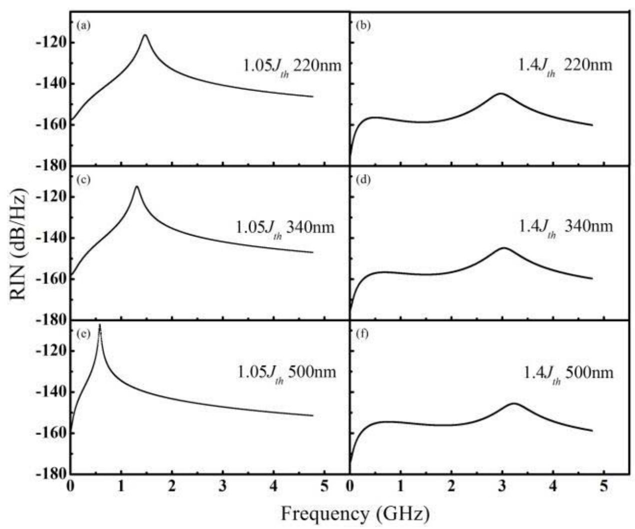

Fig. 4. The RIN spectra for hybrid laser with the same 3μm III-V width, different SOI height under two injection current density levels: (a) Injection current density is 1.05J_{th}, Si ridge height 220nm; (b) Injection current density is 1.4J_{th}, Si ridge height 220nm; (c) Injection current density is 1.05J_{th}, Si ridge height 340nm; (d) Injection current density is 1.4J_{th}, Si ridge height 340nm; (e) Injection current density is 1.05J_{th}, Si ridge height 500nm; (f) Injection current density is 1.4J_{th}, Si ridge height 500nm.

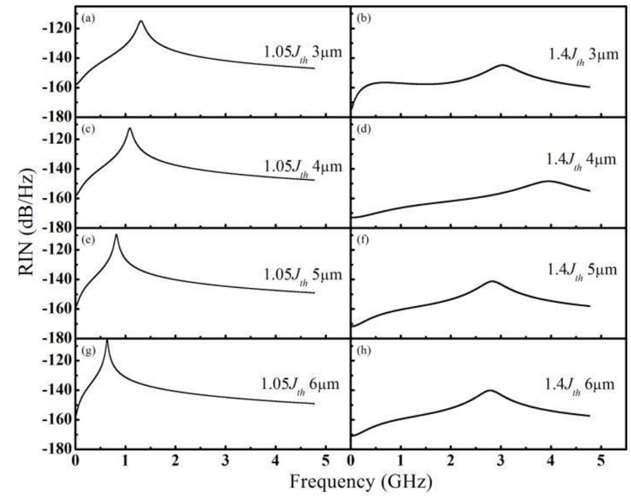

Fig. 5. The RIN spectra for hybrid laser with same SOI height 340nm, different III-V width under two injection current density levels: (a) Injection current density is 1.05J_{th}, 3μm III-V width; (b) Injection current density is 1.4J_{th}, 3μm III-V width; (c) Injection current density is 1.05J_{th}, 4μm III-V width; (d) Injection current density is 1.4J_{th}, 4μm III-V width; (e) Injection current density is 1.05J_{th}, 5μm III-V width; (f) Injection current density is 1.4J_{th}, 5μm III-V width; (g) Injection current density is 1.05J_{th}, 6μm III-V width; (h) Injection current density is 1.4J_{th}, 6μm III-V width.

The confinement of cavity mode in active region will follow the variation of Si ridge height. The effect of Si ridge height on the RIN is shown in Fig. 4. It can be seen that when only the TE_{00} mode is excited at 1.05J_{th}, as the Si ridge height increases, the RO frequency is redshifted and the peak value of RIN increases. However, when both TE_{00} and TE_{10} modes are excited at 1.4J_{th}, as the Si ridge height increases, RO frequency is blueshifted and the peak value of RIN decreases. Moreover, one of the peaks is gradually suppressed. It could be attributed to the variation of cavity mode profile in the hybrid laser. As shown in Fig. 1, a part of TE_{00} mode excited in the III-V waveguide couples into the SOI and the maximum intensity in III-V waveguide is located at the center of ridge. However, for the TE_{10} mode, the confinement in SOI is very small and the maximum intensity in III-V is located away from the center of ridge. Therefore, the overlap of cavity modes TE_{00} and TE_{10} is low so as to induce a low RIN at low frequency range [15]. As Si ridge height increases, confinement of TE_{00} mode in SOI is even higher and the mode overlap of the TE_{00} and TE_{10} modes is further reduced. Therefore, the first peak at low frequency range is further suppressed.

The III-V ridge dimension design can also influence the mode distributions in hybrid lasers hence the RIN, as shown in Fig. 5. As the III-V ridge width increases, if only TE_{00} mode is excited, the RO frequency is redshifted and the peak value of RIN increases. However, when both TE_{00} and TE_{10} modes are excited, the RO frequency is firstly blueshifted then redshifted and the peak value firstly decreases then increases. It shows us that, in our calculation, a 4μm width design has the highest RO frequency and the minimum peak value of RIN. This indicates a theoretically optimum III-V ridge width for the maximum modulation bandwidth and the lowest RIN with fixed 340nm Si ridge height. It is noted that for a fixed Si ridge height of 220nm, the RIN shows the same characteristic by changing the III-V ridge widths. These characteristics could be attributed to the ratio of confinement in active region to ridge area (ridge width $\times$ cavity length). It is experimentally found that it is not the confinement in quantum wells for conventional MQW lasers but the ratio of confinement to ridge area [13] which determines the RO frequency: the larger the ratio, the higher the frequency. In our calculations, as the III-V ridge width increases, the ratio first increases then decreases; therefore, the peak of RIN shows an optimum value. In addition, the first peak of the RIN spectrum is gradually suppressed as the III-V ridge width increases due to the lower and lower overlap of the TE_{00} and TE_{10} modes.

We will close our analysis by comparing the RIN spectrum of a hybrid laser with that of a conventional MQW laser with

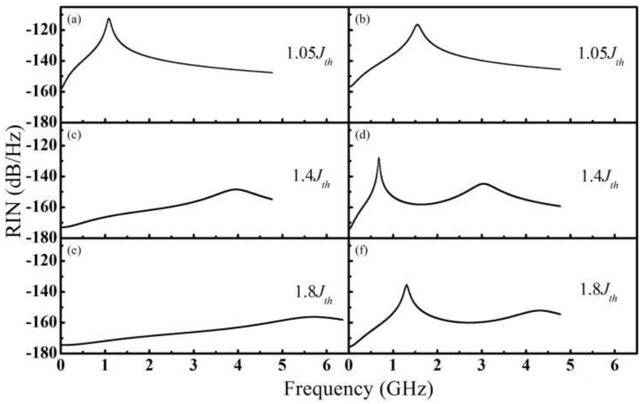

Fig. 6. Comparison of the RIN spectra for a hybrid laser (a) (c) (e) and diode laser (b) (d) (f) with same ridge width of 4μm, under different injection current densities: Injection current density is 1.05J_{th} (first row); Injection current density is 1.4J_{th} (second row); Injection current density is 1.8J_{th} (third row).

same epitaxial structures, as shown in Fig. 6. The III-V ridge widths for both lasers are 4μm and Si ridge in the hybrid laser is 340 nm high. When only TE_{00} mode is excited at 1.05J_{th}, the RIN spectrum of the hybrid laser shows a larger peak value and a lower RO frequency than those of the MQW laser, which is due to the lower confinement in active regions in hybrid laser [19]. In contrast, when both TE_{00} and TE_{10} modes are excited, the first peak at RO frequency is clearly observed for the MQW laser, while the hybrid laser shows a nearly disappeared peak at the RO frequency, because the mode overlap between the two modes is very small in the hybrid laser. Furthermore, the second RO frequency of the MQW laser is lower than that of the hybrid laser. Our simulation result, as shown in Fig. 6(b), on the RIN for conventional MQW lasers can match well with the experimental values [20]. In addition, the simulated modulation bandwidth derived from the RIN spectrum of hybrid lasers is also comparable to the experimental modulation bandwidth [21]. The small discrepancy can be attributed to the gain saturation effect [18], which is not considered in this simulation for the sake of simplification. These results indirectly verify the model we proposed.

In terms of application of a laser system, noise floor level is also very important. Laser intensity noise, as one of the major noise sources, limits the application for high speed modulation system. When silicon hybrid laser is operated with high injection currents, our simulation results show that the noise level is close to the standard quantum limit which is $2h\nu/P_0 = -170.68$dB/Hz (with an output power of 30mW). In addition, our calculation shows that hybrid lasers have a similar noise level compared with conventional diode lasers. This result indicates that silicon hybrid laser is suitable as a source for high fidelity optical transmission.

VI. Conclusion

In this work, we theoretically investigate the RIN spectra of hybrid lasers considering the two-dimension transverse mode profiles. It shows that when only one transverse mode is excited, the RIN spectrum of the hybrid laser shows a larger peak value at RO frequency but a lower RO frequency than those of the MQW laser with the same ridge width. When two transverse modes are excited, the laser system shows two RO frequencies. In this case, the hybrid laser shows a lower peak value at RO frequency and a higher RO frequency than those of the MQW laser. The effects of Si ridge heights and III-V ridge widths on the RIN are also studied in details. Specifically, as Si ridge height increases, when only TE_{00} mode is excited, the RO frequency is red-shifted and the peak value of RIN increases; however, when both TE_{00} and TE_{10} modes are excited, RO frequencies are blue-shifted and the peak value of RIN decreases. In addition, as the III-V ridge width increases, when only TE_{00} mode is excited, the RO frequency is red-shifted and the peak value of RIN increases; however, when both TE_{00} and TE_{10} modes are excited, the RO frequency is firstly blue-shifted then red-shifted and the peak value first decreases then increases. The investigations on the RIN spectra of the hybrid laser show an associated theoretical maximum modulation bandwidth of the device.

The presented model can well reflect the noise characteristics of hybrid lasers to some extent and enable a fast prediction and optimization of device performance. However, there are still certain aspects that the model can be further improved. The most important issues, which should be taken into account for more accurate calculations, are to include gain saturation and heat effect. The lack of gain saturation will overestimate the RO frequency, and lack of heat effect will assume constant structure parameters and underestimate the noise floor level. This requires a further investigation.

References

[1] F. Ellinger, "26–42 GHz SOI CMOS low noise amplifier," *IEEE J. Solid-State Circuits*, vol. 39, no. 3, pp. 522–528, Mar. 2004.

[2] R. Soref, "The past, present and future of silicon photonics," *IEEE J. Sel. Topics Quantum Electron.*, vol. 12, no. 6, pp. 1678–1687, Dec. 2006.

[3] H. Rong *et al.*, "A continuous-wave Raman silicon laser," *Nature*, vol. 433, pp. 725–728, Feb. 2005.

[4] S. Lombardo, S. U. Campisano, G. N. van den Hoven, A. Cacciato, and A. Polman, "A room-temperature luminescence from Er^{3+}-implanted semi-insulating polycrystalline silicon," *Appl. Phys. Lett.*, vol. 63, no. 14, pp. 1942–1944, 1993.

[5] A. W. Fang, H. Park, O. Cohen, R. Jones, M. J. Paniccia, and J. E. Bowers, "Electrically pumped hybrid AlGaInAs-silicon evanescent laser," *Opt. Exp.*, vol. 14, no. 20, pp. 9203–9210, 2006.

[6] A. W. Fang *et al.*, "Integrated AlGaInAs silicon evanescent race track laser and photodetector," *Opt. Exp.*, vol. 15, no. 5, pp. 2315–2322, 2007.

[7] A. W. Fang, E. Lively, Y.-H. Kuo, D. Liang, and J. E. Bowers, "A distributed feedback silicon evanescent laser," *Opt. Exp.*, vol. 16, no. 7, pp. 4413–4419, 2008.

[8] B. R. Koch, A. W. Fang, O. Cohen, and J. E. Bowers, "Mode-locked silicon evanescent lasers," *Opt. Exp.*, vol. 15, no. 18, pp. 11225–11233, 2007.

[9] A. W. Fang *et al.*, "A racetrack mode-locked silicon evancescent laser," *Opt. Exp.*, vol. 16, no. 2, pp. 1393–1398, 2008.

[10] H. Park *et al.*, "A hybrid AlGaInAs-silicon evanescent preamplifier and photodetector," *Opt. Exp.*, vol. 15, no. 21, pp. 13539–13546, 2007.

[11] H. Park, A. W. Fang, R. Jones, O. Cohen, M. J. Paniccia, and J. E. Bowers, "A hybrid AlGaInAs-silicon evanescent waveguide photodetector," *Opt. Exp.*, vol. 15, no. 10, pp. 6044–6052, 2007.

[12] G. P. Agrawal and N. K. Dutta, *Semiconductor Lasers*, 2nd ed. New York, NY, USA: Van Nostrand, 1993.

[13] M. C. Tatham, I. F. Lealman, C. P. Seltzer, L. D. Westbrook, and D. M. Cooper, "Resonance frequency, damping, and differential gain in 1.5 m multiple quantum-well lasers," *IEEE J. Quantum Electron.*, vol. 28, no. 2, pp. 408–414, Feb. 1992.

[14] M. Faugeron *et al.*, "High-power, low RIN 1.55-μm directly modulated DFB lasers for analog signal transmission," *IEEE Photon. Technol. Lett.*, vol. 24, no. 2, pp. 116–118, Jan. 15, 2012.

[15] A. Valle and L. Pesquera, "Theoretical calculation of relative intensity noise of multimode vertical-cavity surface-emitting lasers," *IEEE J. Quantum Electron.*, vol. 40, no. 6, pp. 597–606, Jun. 2004.

[16] B. B. Bakirb *et al.*, "Electrically driven hybrid Si/III–V Fabry–Pérot lasers based on adiabatic mode transformers," *Opt. Exp.*, vol. 19, no. 11, pp. 10317–10325, 2011.

[17] X. Sun, H.-C. Liu, and A. Yariv, "Adiabaticity criterion and the shortest adiabatic mode transformer in a coupled-waveguide system," *Opt. Lett.*, vol. 34, no. 3, pp. 280–282, 2009.

[18] K. Petermann, *Laser Diode Modulation and Noise*. Amsterdam, The Netherlands: Kluwer, 1988, ch. 7.

[19] C. B. Su and V. A. Lanzisera, "Ultra-high-speed modulation of 1.3-μm InGaAsP diode lasers," *IEEE J. Sel. Topics Quantum Electron.*, vol. QE-22, no. 9, pp. 1568–1578, Sep. 1986.

[20] A. M. Millard, "High speed modulation of semiconductor lasers and properties of silver-coated quantum-dot lasers," Ph.D. dissertation, Dept. Electr. Comput. Eng., Univ. Illinois at Urbana-Champaign, Urbana, IL, USA, 2010.

[21] J. R. Heck *et al.*, "Hybrid silicon photonics for optical interconnects," *IEEE J. Sel. Topics Quantum Electron.*, vol. 17, no. 2, pp. 333–346, Apr. 2011.

Xiao Nan Hu received the B.Eng. (Hons.) degree from the School of Electrical and Electronics Engineering, Nanyang Technological University, Singapore, in 2012, where he is currently pursuing the Ph.D. degree. His research interests are in the area of semiconductor lasers and silicon hybrid lasers.

Tao Liu received the B.Eng. degree from Hainan University and the M.Eng. degree from the South China University of Technology in 2007 and 2010, respectively. He is currently pursuing the Ph.D. degree with the School of Electrical and Electronics Engineering, Nanyang Technological University, Singapore. His research interests are in the area of laser theory, and many-body and light-matter interactions in low-dimensional materials.

Yu Lian Cao received the Ph.D. degree from the Institute of Semiconductors, Chinese Academy of Sciences, Beijing, China, in 2006. Her thesis was on the fabrication and characterization of quantum dot and quantum well lasers. She is currently an Associate Professor at the Institute of Semiconductors, Chinese Academy of Sciences, Beijing. Since 2012, she has been a Research Fellow involved in hybrid silicon lasers and optical amplifiers with the School of Electrical and Electronic Engineering, Nanyang Technological University, Singapore. Her current research interests include the quantum-dot lasers, type-II InAs/GaSb superlattice infrared photodetectors, and other optoelectronic devices.

Bo Meng received the B.S. degree in optical information science and technology from Harbin Engineering University, Harbin, China, and the M.S. degree from the Harbin Institute of Technology, Harbin, in 2007 and 2009, respectively. He is currently pursuing the Ph.D. degree in microelectronics with the School of Electrical and Electronic Engineering, Nanyang Technological University, Singapore. His current research interests include the development of tunable single mode quantum cascade laser devices, physics and modulation of semiconductor lasers, midinfrared plasmonics, and microfabrication.

Hong Wang received the B.Eng. degree from Zhejiang University, Hangzhou, China, and the M.Eng. and Ph.D. degrees from the Nanyang Technological University (NTU), Singapore, in 1988, 1998, and 2001, respectively, where he is currently an Associate Professor with the School of Electrical and Electronic Engineering. Before he joined NTU in 1996, he was with the Institute of Semiconductors, Chinese Academy of Sciences, from 1988 to 1994, where he developed InP-based optoelectronic integrated circuits. From 1994 to 1995, he was a Royal Research Fellow with British Telecommunications Laboratories, Ipswich, U.K., where he was involved with the development of InP-based heterostructure field-effect transistors using E-beam lithography.

Dr. Wang was a recipient of the Royal Research Fellowship, U.K., from1994 to 1995, and a co-recipient of the 2007 Defense Technology Prize, MINDEF, Singapore, for his outstanding contributions to the development of MMICs. His current research interests include III–V devices and technology, micro and nanofabrication, RF Si MOS devices and technologies, and RF MEMS.

Geok Ing Ng received the Ph.D. degree in electrical engineering from the University of Michigan, Ann Arbor, in 1990. From 1991 to 1993, he was a Research Fellow at the Centre for Space Terahertz Technology, University of Michigan, involved in microwave/millimeter-wave semiconductor devices and MMICs. In 1993, he joined TRW Inc., Space Park, CA, USA, as a Senior Member of Technical Staff involved in the research and development work on GaAs- and InP-based HEMTs for high-frequency low-noise and power MMIC applications. In 1995, he joined Nanyang Technological University (NTU) as a Lecturer. In 1996, he became a Senior Lecturer and was seconded to be the Program Manager for the III–V MMICs Program at the Microelectronics Centre, NTU. He is currently an Associate Professor at NTU and the Head of the Division of Microelectronics, School of Electronics and Electrical Engineering, and is seconded to Temasek Laboratories at the Nanyang Technological University as a Program Manager for the MMIC Design Centre. His current research interests include device physics, fabrication, and characterization of microwave devices with different III–V material systems for low-noise, power and MMIC applications, and MEMS.

In 1990, he was awarded the European Microwave Prize for his work on InP-based heterostructure monolithic amplifiers.

Xian Shu Luo received the M.S. and Ph.D. degrees from the Institute of Semiconductors, Chinese Academy of Sciences, Beijing, China, and the Hong Kong University of Science and Technology, Hong Kong, in 2006 and 2010, respectively.

He joined the Institute of Microelectronics, Agency for Science, Technology and Research, Singapore, as a Scientist, in 2010. He is currently involved in the optoelectronics, nanophotonics, and silicon-based integrated photonics.

Tsung Yang Liow received the B.Eng. and Ph.D. degrees in electrical and computer engineering from the National University of Singapore (NUS), Singapore, in 2003 and 2008, respectively.

At NUS, he was involved in the design and fabrication of sub-10-nm FinFETs and nanowire transistors. He is currently a Research Scientist with the Institute of Microelectronics, Agency for Science, Technology and Research (A*STAR), Singapore, involved in silicon photonic components and circuits.

Dr. Liow received the NUS Faculty of Engineering Innovation Award in 2003, the A*STAR Graduate Scholarship in 2004, and the President's Technology Award in 2010.

Jun Feng Song received the M.S. and Ph.D. degrees from the College of Electronic Science and Engineering, Jilin University, Changchun, China, in 1996 and 2000, respectively.

He became a Professor at Jilin University in 2005. He joined the Institute of Microelectronics, Agency for Science, Technology and Research, Singapore, in 2006. He is currently involved in the optoelectronics, nanophotonics, silicon-based integrated photonics, and semiconductor lasers.

Guo Qiang Lo (M'08) received the M.S. and Ph.D. degrees in electrical and computer engineering from the University of Texas at Austin, Austin, in 1989 and 1992, respectively. He was with Integrated Device Technology, Inc., in both San Jose, CA, USA, and Hillsboro, OR, USA, involved in Si-semiconductor manufacturing areas in process and integration module research and development. Since 2004, he has been with the Institute of Microelectronics (IME), Agency for Science, Technology and Research, Singapore. He is currently the Laboratory Director for IME's Semiconductor Process Technology and the Program Director of Nanoelectronics and Photonics program. He has authored and co-authored more than 100 peer-reviewed journal and conferences publications, and more than 20 granted U.S. patents. His research interests are in novel semiconductor device and integration technology, in particular, nanoelectronics devices and Si microphotonics.

Dr. Lo was a recipient of the IEEE George E. Smith Award in 2008 for the Best Paper Published in IEEE ELECTRONIC DEVICE LETTERS in 2007.

Qi Jie Wang (M'10–SM'10) received the B.E. degree in electrical engineering from the University of Science and Technology of China, Hefei, China, in 2001, graduating one year in advance, and the Ph.D. degree in electrical and electronic engineering from Nanyang Technological University (NTU), Singapore, in 2005, with NTU and Singapore Millennium Foundation (SMF) scholarship. He received the 2005 SMF Post-Doctoral Fellowship at NTU. Then, he joined the School of Engineering and Applied Science, Harvard University, with Prof. Federico Capasso's group as a Post-Doctoral Researcher in 2007. In 2009, he was assigned as a Joint Nanyang Assistant Professor at the Microelectronics Division, School of Electrical and Electronic Engineering, and the Physics and Applied Physics Division, School of Physical and Mathematical Sciences.

His current research interests are to explore theoretically and experimentally nanostructured semiconductor and fiber-based materials, and nanophotonic devices (nanoplasmonics, photonic crystals, and metamaterials) with an emphasis on all aspects of the problem from design, fabrication, and characterization to integration at system level.

He was a recipient of the top prize for the Young Inventor Awards of the SPIE Photonics Europe Innovation Village in 2004, a golden award from the Fifth Young Inventor's Awards from *HP and Wall Street Journal* in 2005, and a co-recipient of the Institution of Engineers Singapore Prestigious Engineering Achievement Team Award of Singapore in 2005.